



HAL
open science

Airborne gravity reveals interior of Antarctic volcano

T.A. Jordan, F. Ferraccioli, P.C. Jones, J.L. Smellie, M. Ghidella, H. Corr

► **To cite this version:**

T.A. Jordan, F. Ferraccioli, P.C. Jones, J.L. Smellie, M. Ghidella, et al.. Airborne gravity reveals interior of Antarctic volcano. *Physics of the Earth and Planetary Interiors*, 2009, 175 (3-4), pp.127. 10.1016/j.pepi.2009.03.004 . hal-00535572

HAL Id: hal-00535572

<https://hal.science/hal-00535572>

Submitted on 12 Nov 2010

HAL is a multi-disciplinary open access archive for the deposit and dissemination of scientific research documents, whether they are published or not. The documents may come from teaching and research institutions in France or abroad, or from public or private research centers.

L'archive ouverte pluridisciplinaire **HAL**, est destinée au dépôt et à la diffusion de documents scientifiques de niveau recherche, publiés ou non, émanant des établissements d'enseignement et de recherche français ou étrangers, des laboratoires publics ou privés.

Accepted Manuscript

Title: Airborne gravity reveals interior of Antarctic volcano

Authors: T.A. Jordan, F. Ferraccioli, P.C. Jones, J.L. Smellie,
M. Ghidella, H. Corr

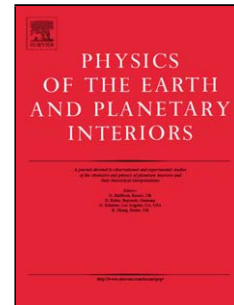
PII: S0031-9201(09)00058-2
DOI: doi:10.1016/j.pepi.2009.03.004
Reference: PEPI 5152

To appear in: *Physics of the Earth and Planetary Interiors*

Received date: 25-3-2008
Revised date: 18-2-2009
Accepted date: 6-3-2009

Please cite this article as: Jordan, T.A., Ferraccioli, F., Jones, P.C., Smellie, J.L., Ghidella, M., Corr, H., Airborne gravity reveals interior of Antarctic volcano, *Physics of the Earth and Planetary Interiors* (2008), doi:10.1016/j.pepi.2009.03.004

This is a PDF file of an unedited manuscript that has been accepted for publication. As a service to our customers we are providing this early version of the manuscript. The manuscript will undergo copyediting, typesetting, and review of the resulting proof before it is published in its final form. Please note that during the production process errors may be discovered which could affect the content, and all legal disclaimers that apply to the journal pertain.



1 **Airborne gravity reveals interior of Antarctic volcano**

2 T. A. Jordan^{*1}, F. Ferraccioli¹, P.C. Jones^{1,2}, J.L. Smellie¹, M. Ghidella³, H. Corr¹

3 ¹ British Antarctic Survey, High Cross, Madingley Road, Cambridge, CB3 0ET,

4 UK

5 ² Now at: ARKeX Ltd. Newton House, Cambridge Business Park, Cambridge,

6 CB4 0WZ, UK

7 ³ Instituto Antártico Argentino Cerrito 1248, 1010 Buenos Aires, Argentina

8

9 **Abstract**

10 Understanding Antarctic volcanoes is important as they provide a window on
11 magmatic and tectonic processes of the Antarctic plate and contain datable records of
12 ice-sheet changes. We present the results from the first detailed airborne radar and
13 gravity surveys across James Ross Island, northern Antarctic Peninsula, which is
14 dominated by Mt Haddington, an ice-covered Miocene-Recent alkaline stratovolcano.
15 The surveys provide new insights into the subsurface structure of the volcano and
16 hence its development, which are unavailable from the surface geology alone. We
17 show that Mt Haddington is associated with a significant negative Bouguer gravity
18 anomaly (< -26 mGal), which suggests that there has not been significant pooling and
19 solidification of a dense shallow-level mafic magma chamber during the growth of the
20 volcano over at least the past 6 m.y., which is consistent with independent
21 geochemical evidence. Simple flexural isostatic models cannot explain the localised
22 negative Bouguer anomaly. 3D modelling techniques show that the negative anomaly
23 is best explained by a shallow, low-density intra-crustal body with its top close to, or

* Corresponding author.

Email address: tomj@bas.ac.uk (T. A. Jordan).

24 at, the surface. Although comparable gravity anomalies are commonly associated
25 with large (~20 km) ash-filled calderas, as seen at Yellowstone or Toba, there is no
26 geological evidence on James Ross Island for a similar structure. We therefore
27 propose that the James Ross Island volcanic edifice subsided into the thick underlying
28 pile of relatively soft Jurassic and Cretaceous sediments, which were displaced by
29 low-density hyaloclastite breccia. The type of deformation envisaged is similar to that
30 associated with Concepcioú, or Iwaki volcanoes in South America, although Mt
31 Haddington is much larger.

32

33 *Key words:* Airborne gravity, basaltic volcano, gravitational spreading, Antarctica.

34

35 **1. Introduction**

36 Airborne gravity is becoming an increasingly utilised tool for geophysical exploration
37 because it allows cost-effective assessment of the crustal and lithospheric structure on
38 scales of 10's to 100's of km. In remote and logistically challenging areas, such as
39 the polar regions, airborne gravity is particularly useful, since ground- or ship-based
40 gravity methods are often unfeasible (Bell et al., 1998; Bell et al., 1999; Childers et
41 al., 2001).

42

43 Recent airborne gravity surveys over Antarctica have been applied to a broad range of
44 geological studies including: investigation of the West Antarctic Rift System and
45 associated sedimentary basins (Bell et al., 1998; Bell et al., 1999; Jones et al., 2002);
46 assessment of the crustal architecture of the Transantarctic Mountains (Studinger,
47 2004); analysing continental break up and terrane accretion processes (Ferraccioli et
48 al., 2005; Ferraccioli et al., 2006); and imaging geological boundary conditions for

49 subglacial lakes (Studinger et al., 2003; Studinger et al., 2004; Holt et al., 2006). No
50 airborne gravity study has so far addressed the crustal structure of individual Antarctic
51 volcanoes, due to the relatively coarse spatial resolution of this geophysical technique
52 (typically greater than 15 km). Antarctic volcanoes are, however, amongst the most
53 significant geological features of the continent, since they provide unique insights into
54 Cenozoic tectonics, ice sheet evolution and stability (Blankenship et al., 1993;
55 Behrendt et al., 1998; Hambrey et al., 2008).

56

57 Our study presents the results from the first detailed aerogravity survey across James
58 Ross Island, which is located to the east of northern Antarctic Peninsula (Figure 1).
59 James Ross Island is dominated by a very large ice-covered Miocene-Recent alkaline
60 centre known as the Mt Haddington stratovolcano (Nelson, 1975; Smellie et al.,
61 2008), and is therefore a suitable target for airborne gravity investigations.

62

63 Mt Haddington is the largest basaltic volcanic centre on the western margin of the
64 Larsen (sedimentary) Basin, and it is one of the largest volcanoes in Antarctica
65 (LeMasurier and Thomson, 1990). Several volcanic centres were erupted along the
66 length of the Antarctic Peninsula from late Miocene times (mainly $< c. 7$ Ma), in
67 response to cessation of subduction along the Pacific margin (Hole et al., 1992; Hole
68 and Larter, 1993; Hole et al., 1995). However, unlike all the other centres in the
69 region, Mt Haddington has probably been intermittently active for much of the last 10
70 m.y. (Smellie et al., 2008). The regional crustal structure has been constrained using
71 seismic refraction data (Barker et al., 2003; Janik et al., 2006). However these studies
72 have generally focused on active rifting within Bransfield Strait, while the crustal
73 structure beneath James Ross Island remains much less well known.

74

75 Previous aerogeophysical studies have defined the regional setting (LaBrecque and
76 Ghidella, 1997) and local seismic investigations have provided estimates of the
77 thickness of Jurassic to Cretaceous sedimentary infill in the Larsen Basin (del Valle
78 et al., 1992). However, the upper crustal structure beneath the volcanic edifice itself
79 is undescribed. Numerous questions remain about the structure of the volcano interior
80 and, in particular, about the presence or absence of a crustal magma chamber. In this
81 paper we present for the first time our data and interpretations from a collaborative
82 British Antarctic Survey-Instituto Antártico Argentino aerogeophysical survey over
83 James Ross Island. The airborne gravity data and models provide the first
84 geophysical images of the interior of James Ross Island. In particular we reveal the
85 presence of a low-density, shallow-level body beneath Mt Haddington, which we
86 interpret as a volcanic pile dominated by low-density hyaloclastite breccia that has
87 subsided deeply into the underlying Jurassic-Cretaceous sediments of the Larsen
88 Basin.

89

90 **2. Geological and geophysical setting**

91

92 James Ross Island lies within the back-arc Larsen Basin (Elliot, 1998) to the east of
93 the Antarctic Peninsula (Figure 1), which has been the site of ocean-continent
94 convergence since Mesozoic times (Barker, 1982; Larter and Barker, 1991; McCarron
95 and Larter, 1998). Today, subduction only continues at the northern tip of the
96 Antarctic Peninsula at the South Shetland Trench, at a very low rate probably equal to
97 the rate of opening of the Bransfield Strait rift zone (Larter and Barker, 1991;
98 Robertson et al., 2003).

99

100 The crustal thickness beneath the western margin of the Antarctic Peninsula has
101 recently been estimated to be ~ 35 km thick using seismic refraction data (Janik et al.,
102 2006), although previous seismic studies suggested thicknesses of 20-22 km (Barker
103 et al., 2003). Beneath the eastern Antarctic Peninsula there is less information on
104 crustal thickness. However, several studies have been carried out to evaluate the
105 shallow crustal structure of the region. Seismic reflection surveys conducted east of
106 James Ross Island show thick layers of sediment draping the continental margin there
107 (Sloan et al., 1995; Strelin, 1995). Regional airborne gravity and magnetic
108 investigations suggest 5-6 km of sedimentary infill in the Larsen Basin (LaBrecque
109 and Ghidella, 1997), consistent with seismic estimates (del Valle et al., 1992).
110 However, no previous geophysical survey has been able to provide a detailed view of
111 the crustal structure beneath James Ross Island.

112

113 Outcrops on James Ross Island are limited to ice-free areas around the periphery of
114 the island, and the central region, including Mt Haddington, is covered by a
115 permanent ice cap. Volcanic rocks of the James Ross Island Volcanic Group (JRIVG)
116 were erupted from c. 10 Ma (Smellie et al., 2008). They unconformably overlie a
117 Jurassic to late Cretaceous sedimentary succession (Nelson, 1975; Elliot, 1998),
118 which forms the fill of an amagmatic back-arc basin (Larsen Basin). Most of the
119 JRIVG formed since 6.2 Ma and at least 50 mainly effusive eruptions have been
120 documented (Smellie, 1999; Smellie et al., 2008). The JRIVG is a large volcanic field
121 dominated by the very large Mt Haddington stratovolcano, measuring 60-80 km in
122 basal diameter and 1.6 km in summit elevation, together with numerous much smaller
123 satellite centres (Nelson, 1975; Smellie et al., 2008). The volcanic rocks preserve an

124 extensive history of Neogene glacial and interglacial periods (Smellie, 2006; Hambrey
125 et al., 2008; Smellie et al., 2008). Lavas in the group form a sodic alkaline series that
126 is wholly basaltic (basalts—hawaiites) except for minor more evolved (mugearite)
127 segregation veins in rare sills (Nelson, 1975; Smellie, 1987; Sykes, 1989). The basalts
128 closely resemble ocean island basalts (Smellie, 1987; Hole et al., 1992) and the
129 formation of the volcanic field has been explained as a consequence of mantle rising
130 into a crustal “thin-spot” created during limited late Cretaceous-early Tertiary
131 extension (Hole et al., 1992). Such an origin contrasts with the origin of
132 compositionally similar alkaline basalts in other late Miocene and younger outcrops in
133 the Antarctic Peninsula, which formed following the cessation of subduction and
134 development of slab windows (Hole et al., 1992; Hole et al., 1995).

135

136 **3. Survey design and data processing**

137

138 Airborne radar data were collected in 1997/98 as part of a collaborative British
139 Antarctic Survey-Instituto Antártico Argentino survey over James Ross Island. Figure
140 2a shows the surface elevation data derived from our airborne radar and BEDMAP
141 (Lythe et al., 2000), whereas Figure 2b depicts the sub-ice topography beneath the Mt
142 Haddington ice cap. During 1998/99 over 10,000 line-km of aerogeophysical data
143 were collected, including 3,500 line-km of airborne gravity data. Line spacing was 2
144 km, with orthogonal tie lines spaced 10 km apart. Large vertical accelerations were
145 associated with changing altitudes during draped aeromagnetic flights. Hence not all
146 flights yielded usable aerogravity data. Flight line altitudes were constrained by the
147 local topography and were 1050, 1500, 1950, 2050 and 2500 m (Figure 2a).

148

149 Airborne gravity data were collected using a Zero Length Spring Corporation (ZLS) -
150 modified LaCoste and Romberg model S air-sea gravimeter (LaCoste, 1967). The
151 meter was mounted in a gyro-stabilised, shock mounted platform at the centre of mass
152 of the aircraft to minimise the effect of vibrations and rotational motions (Jordan et
153 al., 2007). GPS data were recorded with an Ashtech Z12 dual frequency receiver in the
154 aircraft and at a fixed base station. Differential, carrier phase, kinematic GPS methods
155 were then used to calculate all the navigational information used for the dynamic
156 corrections of the aerogravity data (Mader, 1992).

157

158 Standard processing steps were taken to convert the raw gravity data to free air
159 anomalies (Jones and Johnson, 1995; Jones et al., 2002), including latitude, free air
160 and Eotvos corrections (Harlan, 1968; Woollard, 1979). The vertical accelerations of
161 the aircraft, which dominate the gravity signal recorded by the meter, were calculated
162 by double differencing GPS height measurements (Jones and Johnson, 1995). In
163 addition, a correction was made for gravimeter reading errors caused by the platform
164 tilting when it was subjected to horizontal accelerations (Swain, 1996). After making
165 the above corrections, the data were low pass filtered for wavelengths less than 9 km
166 to remove short wavelength noise from the geological signal. The data were
167 continued to a common altitude of 2050 m (Blakely, 1995) and levelled (Bell et al.,
168 1999). Cross-over analysis at 118 intersections yielded a standard deviation of 2.9
169 mGal, which is within the 1-5 mGal error range typically reported for airborne gravity
170 surveys after levelling (Bell et al., 1999; Jones et al., 2002; Ferraccioli et al., 2005;
171 Ferraccioli et al., 2006; Holt et al., 2006). Comparison between airborne
172 measurements and previous land-based gravity data (Garrett, 1990), yielded an RMS

173 difference of ~ 4.5 mGal, which is within the 2 sigma range for airborne gravity data
174 accuracy.

175

176 3.1. *New Bouguer anomaly map*

177 A Bouguer gravity correction was applied to the free air anomaly data (Figure 2c) to
178 remove the gravity effect of the topography, allowing analysis of subsurface density
179 structures in the region. The Bouguer correction was based on a digital elevation
180 model (DEM) derived from a 1:100,000 topographical map of James Ross Island
181 (BAS, 1995) and BEDMAP data (Lythe et al., 2000). Ice thickness data were also
182 derived from BEDMAP, which incorporates the results of our 1997/1998 airborne
183 radar survey (Figure 2a and b). The Bouguer correction for terrain effects was
184 calculated for a flight elevation of 2050 m, to least squares accuracy, using a Gauss–
185 Legendre quadrature (GLQ) integration method (von Frese et al., 1981; von Frese and
186 Mateskon, 1985). For this correction we assumed ice and water densities of 915 kgm^{-3}
187 and 1028 kgm^{-3} , respectively. The rock density was varied, as the bulk of the
188 volcanic edifice is known to consist of lower density rocks than the standard value of
189 2670 kgm^{-3} (Table 1).

190

191 The Bouguer gravity anomaly (Figure 2d), based on a correction density of 2670 kgm^{-3}
192 has a mean value of ~ 54 mGal with values ranging from 8 mGal, beneath Mt
193 Haddington, to > 50 mGal in the surrounding area. The positive background field
194 appears in long wavelength ($> \sim 500$ km) satellite-derived gravity models such as
195 EGM-96 (Lemoine et al., 1998). To enhance signatures arising from local density
196 variations the long wavelength satellite-derived field was subtracted from the Bouguer
197 anomaly, leaving a residual Bouguer anomaly with a mean value of 3.4 mGal. All the

198 references to the Bouguer anomaly that follow include the correction for the long
199 wavelength, satellite derived gravity field.

200

201 To assess the effect of the rock correction density on the recovered Bouguer gravity
202 anomaly a variety of densities were considered ranging from 2670 kgm^{-3} to 2270 kgm^{-3} ,
203 and are shown in Figure 3a. The minimum Bouguer anomaly calculated using a
204 standard rock density of 2670 kgm^{-3} is $\sim -44 \text{ mGal}$ along profile A-A' (Fig. 2d). As
205 the correction density was decreased the negative anomaly associated with James
206 Ross Island is reduced to $\sim -26 \text{ mGal}$, for the minimum correction density of 2270
207 kgm^{-3} .

208

209 To constrain the correction density we considered the lithologies that make up Mt
210 Haddington. The typical volcanic succession is made up of lava-fed deltas 200 to 600
211 m thick (Skilling, 2002; Smellie, 2006; Smellie et al., 2008). These are dominated by
212 hyaloclastite breccias, that make up $\sim 60-75\%$ of the thickness of each delta, and are
213 typically capped by subaerial lava flows. Although tuff cones are also present in the
214 JRIVG, they are uncommon and of limited lateral extent except for that forming
215 Terrapin Hill, on the north side of the island. Average density observations and
216 proportions of the various lithologies are shown in Table 1. Consideration of the
217 densities and proportions of the different lithologies suggests that the bulk mean
218 density of the Mt Haddington volcanic edifice is $\sim 2470 \text{ kgm}^{-3}$ and this value was
219 adopted to calculate the Bouguer anomaly.

220

221 The dominant feature of the Bouguer gravity anomaly in Figure 2d is a prominent
222 negative anomaly centred over Mt Haddington. The anomaly is also co-located with a

223 series of particularly high-amplitude aeromagnetic anomalies, which must relate to
224 volcanic rocks currently obscured by the Mt Haddington ice cap (grey regions in
225 Figure 2d). The first question we address in the following sections is whether the
226 Bouguer gravity low over the island may be related to simple isostatic compensation
227 of the volcano edifice.

228

229 **4. Isostatic compensation**

230

231 At long wavelengths, topographic loads on the lithosphere are supported at depth by a
232 low-density crustal root (Figure 4a), in a similar manner to a floating iceberg (Watts,
233 2001). This compensation deflects the Moho leading to generally negative Bouguer
234 gravity anomalies beneath mountain ranges and positive Bouguer anomalies across
235 continent-ocean transitions and in offshore regions (Watts and Stewart, 1998). For
236 the Airy isostatic model we assumed densities of 1028 kgm^{-3} , 2800 kgm^{-3} , and 3330
237 kgm^{-3} for water, crust and mantle, respectively. The gravity anomaly resulting from
238 the Airy isostatic model was calculated using the Gauss- Legendre quadrature (GLQ)
239 method (von Frese et al., 1981), assuming an observation altitude of 2050 m. The
240 crustal thickness for topography at sea level (T_i in Figure 4a) is an important
241 additional assumption when calculating the isostatic anomaly. However, it is not well
242 known for James Ross Island. For this investigation, we considered two values of 22
243 and 35 km for initial crustal thicknesses, to show the impact of the reference Moho
244 depth.

245

246 Figure 3a shows the positive gradient of the Bouguer gravity anomaly in the east of
247 the region matches that predicted from Airy isostatic compensation close to the

248 continent-ocean transition. LaBrecque and Ghidella (1997) had previously noted this
249 feature from regional airborne gravity data. Part of the negative Bouguer anomaly in
250 the western survey region may also be explained in terms of simple Airy isostatic
251 compensation of the surface topography in the Antarctic Peninsula. The impact of
252 increasing the initial crustal thickness from 22 km to 35 km is to reduce the amplitude
253 of the short wavelength anomalies caused by isostatic deflection of the Moho.
254 However, both values of initial crustal thickness give a good fit to the regional
255 gradient.

256

257 Previous authors, such as Watts (2001), have shown that topographic loads may be
258 supported, in part, by the elastic rigidity of the lithosphere. This leads to less
259 deflection beneath the load, and the development of a flexural moat, beyond the load
260 edge, as shown in Figure 4b. The extent of elastic support of a topographic load can
261 be assessed based on comparison of calculated gravity anomalies, derived from
262 simple elastic models, with the observed Bouguer anomaly. The technique recovers
263 the equivalent elastic thickness (T_e) that best represents the integrated strength of the
264 lithosphere. In the case of the flexural isostatic models considered in this study the
265 gravity effect of both the deflection of the Moho, and the development of a flexural
266 depression filled with lower density infill were considered (Figure 4b).

267

268 A series of flexural models were constructed to assess the style of crustal
269 compensation of the volcanic load on James Ross Island. These models used the
270 GMT (Generic Mapping Tool) routine `grdfft` (Wessel and Smith, 1991) to
271 calculate the expected flexure, assuming a continuous elastic plate model. The load
272 distribution was based upon the spatial distribution of high-frequency aeromagnetic

273 anomalies, which matches the mapped outcrop pattern of both the volcanic formations
274 and the Cretaceous sediments (Nelson, 1975). The effect of the Mt Haddington ice
275 cap was included in the calculation by converting the ice thickness into ‘equivalent
276 rock thickness’ by correcting for ice density. Load and infill densities used in the
277 flexural model were 2470 kgm^{-3} , mantle density was assumed to be 3330 kgm^{-3} , and
278 the load was assumed to be displacing air.

279

280 The gravity anomalies derived from the flexural models were calculated using the
281 GLQ method (von Frese et al., 1981). The gravity model assumed the existence of
282 two interfaces, the first between the sedimentary infill and the crust, and the second at
283 the Moho. The Moho reference depth was assumed to be 22 km. However, the Moho
284 reference depth has little impact on the calculated gravity anomaly pattern as most of
285 the signal is derived from the low-density infill in the flexural depression. For the
286 gravity calculation, the same densities were used as in the flexural model, and a
287 crustal density of 2800 kgm^{-3} was assumed. The model observation elevation was
288 2050 m, coincident with the upward continued flight level.

289

290 4.1 Results of the isostatic model

291

292 The driving load and flexural surfaces calculated for various T_e values are shown in
293 Figure 3b. For T_e values between 1 and 4 km flexural subsidence of between 250 and
294 550 m is modelled at the margins of the island. Associated with this subsidence the
295 maximum dip of the flexural surface is between 8.5° and 1.5° towards the centre of
296 the island. Geological observations around James Ross Island, however, do not

297 appear to show any systematic radially-inward dip of the Cretaceous sedimentary
298 strata, or the overlying volcanic strata, towards the centre of the island (Nelson, 1975).

299

300 The gravity anomaly calculated from an Airy isostatic model (i.e. $T_e = 0$ km),
301 including the effect of the low-density infill (Figure 3c), overestimates the amplitude
302 and wavelength of the negative gravity anomaly, relative to the observed Bouguer
303 anomaly. Higher T_e values give a closer match to the amplitude of the observed
304 negative anomaly. The wavelength of the calculated anomaly, however, significantly
305 exceeds that observed, which is localised beneath Mt Haddington. For T_e values >16
306 km the calculated anomaly is ~ -7 mGal beneath the centre of the island and is very
307 broad.

308

309 The results of our flexural modelling studies around James Ross Island suggest that no
310 isostatic model provides a good match with either the gravity or the geological
311 observations. The observed gravity low over James Ross Island is therefore related to
312 an intracrustal low-density body, which is further investigated with 3D inversion
313 techniques.

314

315 **5. 3D inversion**

316 *5.1. Inversion with no a-priori assumptions*

317 The inversion program GRAV3D from the University of British Columbia
318 (GRAV3D, 2006) was applied to constrain the crustal structure of James Ross Island
319 (Figure 5). This technique minimises an objective function of the density model,
320 constrained so that the misfit between the calculated and observed anomaly is within
321 the expected error bounds (Li and Oldenburg, 1998). The objective function defines

322 the smoothness of deviations from a reference model of the density structure. This
323 model was defined as a 3D mesh 100 km wide and 15 km deep, where each cell was 5
324 km wide and 0.5 km deep. The default objective function was used for recovery of the
325 density structure, and results were returned as deviations from an initial reference
326 density of 0 kgm^{-3} . A standard error value of 2.5 mGal was used in the objective
327 function, as this was close to the observed crossover error of the free-air data, and the
328 observation altitude was set at 2050 m.

329

330 The results of the GRAV3D inversion suggest the presence of a low-density body
331 centred at a depth of 3-5 km beneath James Ross Island (Figure 5). The region of rock
332 with an apparent density $< -30 \text{ kgm}^{-3}$ below the background is approximately 15 km
333 across and 15 km thick (Figure 5b). However, the core of this low density region,
334 with an apparent density $< -100 \text{ kgm}^{-3}$ below the background, is between 0.5 and 9.5
335 km depth (Figure 5c,d). The predicted gravity structure based on this inversion
336 technique has a similar pattern to the observed Bouguer anomaly. However, the
337 amplitude of the negative anomaly predicted by the 3D inversion underestimates the
338 observed anomaly by $\sim 15 \text{ mGal}$. This is likely due to the default objective function
339 used in GRAV3D, which prevents the introduction of abrupt density changes
340 associated with the Mt Haddington volcano edifice. However, geologically such
341 variability is likely to occur.

342

343 5.2 *Constrained inversion*

344

345 An alternative to applying an inversion with no a-priori constraints is to make
346 assumptions about the low-density body. In the present example, such assumptions

347 include the depth to the top of the source body and the apparent density contrast with
348 respect to background values.

349

350 Our first model considered the top of the body to be at zero metres elevation and the
351 low-density body was assumed to be displacing upper crustal rocks with an apparent
352 density of 2670 kgm^{-3} . We refer to this model as the “caldera-like” model. The
353 apparent density for the caldera-like body was assumed to be $\sim 2370 \text{ kgm}^{-3}$. This is
354 lower than the mean density assumed for the volcanic edifice itself (Table 1).
355 However, using a body density of 2470 kgm^{-3} would result in an unrealistic caldera-
356 like body-thickness of over 12 km. There is some geological evidence for a somewhat
357 lower density volcanic pile: Because subglacial eruptions on Mt Haddington would
358 have typically commenced with construction of a subaqueous tuff cone (cf. Smellie,
359 2000), multiple eruptions in the summit region would have produced a relatively deep
360 core of lower density hyalotuff (Table 1), thus reducing the overall density of the
361 edifice.

362

363 In the second model the top of the source body was placed at depth. We refer to this
364 model as the “magma chamber” model. In this model magma was assumed to ‘pond’
365 within the crust at the level of neutral buoyancy (Walker, 1989), which we assumed
366 was at the base of the sedimentary sequence. For the gravity calculations the density
367 of the magma was assumed to be 2670 kgm^{-3} , which is at the lower end of the range
368 suggested for basaltic magma (Walker, 1989; Dufek and Bergantz, 2005). The
369 overlying sediment was assumed to have a density of 2670 kgm^{-3} . The magma
370 chamber was modelled as intruding basement rock with a density of 2800 kgm^{-3} .
371 Aeromagnetic and seismic estimates yield a thickness of 5-6 km of Jurassic and

372 Cretaceous sediments in the James Ross Island region (del Valle et al., 1992;
373 LaBrecque and Ghidella, 1997). The top of the “magma chamber” body was
374 therefore placed at 5 km depth.

375

376 To estimate the size of the low-density body beneath James Ross Island the negative
377 component of the Bouguer anomaly was considered. The initial body size (t) was
378 derived from the simple Bouguer slab formula, $g_{obs}=2\pi G\Delta\rho t$, where g_{obs} is the
379 observed gravity anomaly, G is the universal gravitation constant and $\Delta\rho$ is the
380 density contrast between the body and the background. The gravity anomaly resulting
381 from the initial body was calculated using the GLQ method (von Frese et al., 1981).
382 The residual between the calculated anomaly and negative Bouguer anomaly was then
383 used to adjust the body size. This process was continued until the change in the
384 calculated gravity anomaly after each iteration was less than 2.9 mGal (the r.m.s.
385 measurement error).

386

387 Figures 6a and b show that the “caldera model” can provide a reasonable fit to the
388 observed gravity data if the body is 6.5 km thick. The simple “magma chamber”
389 model with its top at 5 km depth (Figures 6 c and d) cannot account for the observed
390 anomaly, as the wavelength of the calculated anomaly is significantly broader (~40
391 km) than the ~20 km wide observed anomaly. In addition, the thickness of the magma
392 chamber would have to approach the assumed crustal thickness in the region, making
393 the model geologically unrealistic. A shallow caldera-like body is therefore our
394 preferred model for the causative body. However, the observed anomaly may result
395 from a combination of shallow and deep sources. This ambiguity problem cannot be
396 resolved solely from airborne gravity data modelling.

397

398 **6. Discussion**399 *6.1. Isostatic compensation and the structure of James Ross Island*

400 Airy isostatic models, which account for the crustal thickening beneath the Antarctic
401 Peninsula and thinning across the continental margin, fit the regional trend observed
402 in the Bouguer gravity data (Fig 3a). However, those Airy isostatic models do not
403 match the magnitude of the localised negative Bouguer anomaly observed over Mt
404 Haddington in the centre of James Ross Island.

405

406 Flexural isostatic models for the response to localised volcanic loading on James Ross
407 Island (Figure 3b) were also assessed. These models included the gravity effect of
408 low-density material infilling the flexural depression. The flexural isostatic models
409 do not provide a calculated gravity anomaly (Figure 3c) that matches the observed
410 data, as the width of the calculated anomaly is significantly broader than observed. In
411 addition, the expected flexural deflection of 8.5° to 1.5° at the margins of the island is
412 not consistent with the observed dip in outcrops of Cretaceous sediments that underlie
413 the volcanic rocks on the island. If flexure had played a significant part in the
414 evolution of the island then a flexural moat filled with sediments of the same age as
415 the volcano would be expected, as seen for example around the Mt. Erebus volcano,
416 Ross Island, which seismic evidence suggests is surrounded by inward-dipping
417 sediments (Stern et al., 1991; Horgana et al., 2005). In contrast, onshore outcrops and
418 offshore seismic data for the James Ross Island region reveal essentially easterly-
419 younging strata dipping homoclinally at c. 10° (Whitham, 1988; Sloan et al., 1995).
420 However, the lack of young sediments in a flanking moat might be explained if recent
421 regional uplift and glacial erosion have stripped off those sediments.

422

423 *6.2. Origin of the low-density body*

424 Simple elastic flexural isostatic models do not account for the observed localised
425 negative Bouguer gravity anomaly over Mt Haddington. A low-density intra-crustal
426 body must therefore be present beneath the island, which we investigated using 3D
427 inversion techniques (section 5). The geological explanation for a low-density body
428 beneath the dominantly basaltic Mt Haddington volcano is not obvious. Felsic
429 volcanism is typically associated with negative Bouguer anomalies caused by the
430 presence of lower density solidified granitic magma chambers, collapsed calderas
431 filled with low density breccias and tuffs, and/or low density hot magma chambers
432 (Lehman et al., 1982; Masturyono et al., 2001; Finn and Morgan, 2002). Examples of
433 negative anomalies associated with felsic volcanism include Yellowstone (Lehman et
434 al., 1982; Finn and Morgan, 2002) and Toba (Masturyono et al., 2001), which both
435 exhibit high-amplitude negative Bouguer anomalies associated with large (>20 km
436 wide) surface calderas filled with pyroclastic tuffs and deeper level low-density
437 magma chambers.

438

439 Conversely, some basaltic volcanoes appear to be associated with negative Bouguer
440 anomalies. For example, Mt Melbourne, an active volcano situated on the western
441 flank of the Ross Sea Rift, is associated with a negative Bouguer anomaly, which
442 might be caused by either (a) low density volcanoclastic material infilling a caldera; or
443 (b) a buried low density body such as a hot magma chamber (Ferraccioli et al., 2000).
444 Marion Island, an active basaltic shield volcano located in the sub-Antarctic Indian
445 Ocean, shows a relatively negative Bouguer anomaly of ~-20 mGal over the centre of
446 the volcanic edifice (Chevallier et al., 1992). Modelling of that anomaly by

447 Chevallier et al. (1992) showed that reasonable configurations of size and density in a
448 low-density magma chamber could not generate the anomaly. Instead, the presence of
449 a 2.5 km-thick low-density body of unknown origin, with a relative density contrast of
450 -500 kgm^{-3} , was proposed beneath the centre of the volcano.

451

452 The ice cap on Mt Haddington is ~ 20 km wide and there is no evidence for a large
453 caldera and associated ash deposits as occur, for example, at Yellowstone and Toba
454 volcanoes (Lehman et al., 1982; Masturyono et al., 2001; Finn and Morgan, 2002).
455 We therefore discount a large-caldera hypothesis for the cause of the observed ~ 20
456 km wide, negative Bouguer anomaly. A smaller caldera structure, perhaps 5 km in
457 diameter and associated with possible sector collapse on the northwest side of Mt
458 Haddington, is suggested by the sub-ice topography close to the summit region
459 (Figure 2b). However, a caldera of that size cannot be the primary cause of the
460 observed longer-wavelength negative Bouguer anomaly.

461

462 A present-day hot magma chamber beneath Mt Haddington cannot be ruled out by
463 airborne gravity data alone, as it could have a neutral density contrast with the
464 surrounding material. However, to produce a negative gravity anomaly, given an
465 expected minimum basaltic magma density of $\sim 2670 \text{ kgm}^{-3}$ (Walker, 1989; Philpotts
466 and Dickson, 2000; Dufek and Bergantz, 2005), the magma chamber would have to
467 be intruding basement rocks, which are known to be below ~ 5 km (del Valle et al.,
468 1992; LaBrecque and Ghidella, 1997). Our modelling shows a hot basaltic magma
469 chamber, at that depth, intruding basement with a density of 2800 kgm^{-3} , cannot
470 account for the observed negative Bouguer anomaly.

471

472 If an intra-crustal magma chamber had previously existed and solidified, earlier in the
473 ~6 Ma eruptive history of the James Ross Island Volcanic Group, a positive Bouguer
474 anomaly would be expected. Such a positive anomaly is not observed, suggesting a
475 significant intra-crustal magma chamber has never existed. This is consistent with
476 geochemical studies, which show no compositional evolution of the eruptive products,
477 and hence no evidence for fractionation within an intra-crustal magma chamber
478 (Nelson, 1975; Smellie, 1987; Sykes, 1989; Hole et al., 1991; Smellie, 1999). The
479 lack of an intra-crustal magma chamber supports the hypothesis that crustal-scale
480 faulting may be allowing melt rapid access to the surface in the region (Smellie, 1987;
481 Smellie, 1999).

482

483 In the absence of a large caldera, another possible geological explanation for the
484 presence of a shallow low-density body beneath Mt Haddington is ductile deformation
485 of the sediments beneath the volcano. Van Wyk De Vries and Matela (1998) used
486 finite-element modelling to show that shallow-level sediments beneath a volcanic load
487 can act as a thin elastic-plastic layer, while deeper sedimentary layers yield by ductile
488 flow. The yielding of the underlying sedimentary basement allows the volcanic
489 edifice to sink into the substrate. This elastic-plastic scenario is shown in Figure 7. In
490 the case of James Ross Island, much of the volcanic edifice is made up of relatively
491 low-density hyaloclastite breccia, which, if it were displacing sediments with a higher
492 density, could generate the observed negative gravity anomaly. In addition, the
493 elastic-plastic model predicts the development of flexural bulges around the volcanic
494 load (van Wyk de Vries and Matela, 1998). Cretaceous basement is exposed at sea
495 level around the periphery of Mt Haddington. In addition, Neogene volcanic units on
496 the west side of James Ross Island and on Vega Island straddle Cretaceous basement

497 “hills” up to 200 m high comparable with elevations of Cretaceous strata on
498 Cockburn, Seymour and Snow Hill islands to the east. The higher basement elevations
499 form an annular outcrop resembling a “bullseye” that encloses Mt Haddington and
500 which might represent a flexural bulge. However, the simple elastic models, shown in
501 Figure 3c, indicate the maximum amplitude of a flexural bulge is small (<50 m).
502 With the substantial bedrock topography on James Ross Island, which is also draped
503 by extensive and seemingly undeformed horizontal lava-fed deltas, it may be difficult
504 to detect visually the presence of any flexural bulge. However, a largely unpublished
505 neotectonic study of the Cretaceous outcrops suggest that a possible annular axis of
506 thrusts and anticlines is located outboard of the main volcanic outcrops (van Wyk de
507 Vries and JL Smellie, unpublished information), which may be related to volcano-
508 induced bedrock spreading (Oehler et al., 2005).

509

510 An elastic-plastic plate model may be an improvement on the purely elastic models
511 considered in Figure 3, because yielding of the plate beneath the large load of Mt
512 Haddington could cause significant localisation of the deformation. The elastic-
513 plastic plate model would explain the narrow width of the observed anomaly,
514 compared to the much broader anomalies predicted by simple constant T_e flexural
515 models. Additional low-density material, either at depth, associated with
516 hydrothermal alteration, or at shallow levels within the volcanic pile, associated with
517 tuff cones, or a small caldera, could increase the amplitude of the localised negative
518 anomaly (Figure 7).

519

520 How the load-induced deformation occurs can be predicted based on the size of the
521 volcanic load, and the thickness and relative viscosity of the ductile layer. In the

522 experiments of van Wyk de Vries and Matela, (1998) thin viscous layers (~1-5 km)
523 lead to spreading of the volcanic edifice, while a thick viscous layer (>>10 km) lead
524 to sinking of the edifice. In the case of James Ross Island, the sediment layer might
525 be as much as ~5 km thick. It is the layer most likely to behave in a ductile manner
526 and lateral spreading of the edifice may be expected to dominate. However, Mt
527 Haddington is between 30 and 50 km wide, rather than 6 km wide, as used in the
528 models of van Wyk de Vries and Matela, (1998). Initial lateral spreading may
529 therefore have created space allowing the central part of the broad volcanic edifice to
530 sink into the sediment. Additionally, the deeper crust may have acted in a viscous
531 manner, as a thick viscous layer, allowing for greater subsidence.

532

533 Lateral spreading of a volcanic edifice may lead to internal deformation of the
534 volcanic edifice and sector collapse (van Wyk de Vries and Francis, 1997; Oehler et
535 al., 2005). The sub-ice topography of Mt Haddington (Figure 2b) shows an arcuate
536 structure, ~5 km in diameter, at the summit of the volcano. This topographic feature
537 could represent evidence for northwest-directed sector collapse of the uppermost part
538 of the volcano, and it leads directly to a postulated flank collapse at the head of Croft
539 Bay, similar to numerous other smaller collapses around the periphery of the volcano
540 (Oehler et al., 2005). A more detailed airborne radar survey could further elucidate the
541 nature of the possible sub-ice collapse structure. If the sub-ice arcuate feature does
542 indeed represent a sector collapse high on the volcano flank, then the pattern of
543 collapse could be similar to that observed on other volcanoes, such as Stromboli
544 (Tibaldi, 2004) or Mombacho (van Wyk de Vries and Francis, 1997) and other
545 oceanic volcanoes characterised by mechanically weak layers, such as hyaloclastite
546 breccias in lava-fed deltas (Oehler et al., 2005). The high level of the putative

547 collapse structure on Mt Haddington may be unique to volcanoes erupted in
548 association with a draping ice sheet since the presence of an ice sheet will ensure that
549 thick hyaloclastite layers (in lava-fed deltas) extend up-dip to near-summit elevations,
550 rather than being restricted to coastal elevations. A structural influence for collapses
551 on Stromboli was suggested since sector collapse has occurred approximately
552 orthogonal to the main trend of dyke intrusion (Tibaldi, 2004). A similar association
553 is suggested for Mt Haddington: (1) the volcano is elliptical in outline, extended more
554 NE—SW than NW—SE, suggesting possible effusion from NE—SW fissures; and
555 (2) collapse scars identified here and by Oehler et al. (2005), indicate landscape
556 rotation and translation directions predominantly to the SE and NW (i.e. orthogonal to
557 the inferred fissure orientation, similar to Stromboli). In addition, the largest and most
558 prominent of the high-amplitude magnetic anomalies on Mt Haddington is also NE—
559 SW aligned and may represent multiple feeder dykes for the volcanism (Fig. 2d).
560 Finally, many of the eruptions from Mt Haddington were extremely voluminous (tens
561 of km³; unpublished information of JL Smellie), consistent with a fissure origin for
562 much of the volcanism.

563

564 Our preferred hypothesis is thus for elastic-plastic deformation induced by volcanic
565 loading. It is supported by unpublished studies of the Cretaceous sediments that form
566 the local bedrock on James Ross Island which are associated with compressional
567 deformation, in the form of low angle thrusts and kink folding (van Wyk de Vries et
568 al., 1992). In future, seismic refraction surveys, across the width of the volcano,
569 could be used to detect and confirm the size and origin of the low density body
570 extending beneath the centre of the island.

571

572 7. **Conclusions**

573

574 Airborne gravity data collected across James Ross Island reveal a prominent negative
575 Bouguer anomaly centred over Mt Haddington, not a positive anomaly typically
576 expected over a basaltic volcano. The lack of a positive Bouguer gravity anomaly
577 suggests that there has never been a significant upper crustal magma chamber. Whilst
578 this may be a surprise for such an unusually long-lived volcanic centre (c. 10 m.y.), it
579 is consistent with the lack of compositional evolution displayed by the volcano, which
580 has erupted only basalts during the entire period.

581

582 Simple Airy or flexural isostatic compensation models cannot account for the negative
583 Bouguer anomaly over the island. The negative Bouguer anomaly was therefore
584 investigated using a variety of 3D inversion techniques, including both an inversion
585 with no a-priori constraints and inversions with fixed depth to top of the source body
586 and apparent density contrasts. Our preferred model explanation is a shallow low-
587 density source body, up to 6 km thick. Gravity modelling over James Ross Island
588 shows that a hot magma chamber cannot account for the amplitude and wavelength of
589 the observed gravity anomaly, and there is no geological evidence for a sufficiently
590 large caldera.

591

592 We propose that loading-induced deformation of the Cretaceous sediments underlying
593 the Mt Haddington volcano has caused the volcanic load to subside deeply into an
594 elastic-plastic sedimentary bedrock. This subsidence replaced the relatively soft
595 Jurassic-Cretaceous bedrock with volcanic units dominated by low-density
596 hyaloclastite breccia, thus creating a shallow, low-density body, the depth of which

597 strongly correlates with the height of the surface volcanic load. Additional low-
598 density hydrothermally altered rocks and/or tuffs might be present but are yet
599 unproven within the central core of the volcano. Their presence, which is geologically
600 reasonable, would further enhance the amplitude of the negative Bouguer gravity
601 anomaly observed. It appears plausible that lateral spreading of the Mt Haddington
602 edifice could promote internal deformation within the volcano and even lead to
603 further potentially hazardous gravitationally driven sector collapse. There is published
604 evidence that such collapses have occurred frequently around the periphery of the
605 volcano in the past, and our study suggests there may be a causal link of those
606 collapses to NW-SE extensional stresses linked to NE-SW aligned fissures.

607

608 Our investigation shows the utility of airborne gravity data as a geophysical tool for
609 probing the interior of ice-covered volcanoes and for identifying and assessing any
610 volcanically-induced crustal loading and deformation processes. Airborne gravity has
611 therefore the potential for becoming a new tool to investigate the structure of several
612 other major subglacial volcanoes and it complements the use of currently more
613 widespread aeromagnetic and airborne radar studies, for example over the glaciated
614 West Antarctic Rift System, which is in parts volcanically active (Corr and Vaughan,
615 2008).

616

617 **Acknowledgments**

618

619 This work is a spin-off from a British Antarctic Survey multidisciplinary investigation
620 that seeks to investigate climate change in Neogene time (ISODYN Project –
621 Icehouse Earth: Stability or Dynamism?). We acknowledge the Instituto Antartico

622 Argentino for providing logistical support for the aerogeophysical survey from
623 Marambio and particularly Pedro Skvarca for help with the airborne radar data. Julie
624 Ferris is thanked for flying the airborne magnetic and gravity survey and we also
625 thank our pilot Giles Wilson from the BAS Air Unit.

626

627 **References**

628

629 Barker, D.H.N., Christeson, G.L., Austin Jr, J.A., and Dalziel, I.W.D., 2003. Backarc
630 basin evolution and cordilleran orogenesis: Insights from new ocean-bottom
631 seismograph refraction profiling in Bransfield Strait, Antarctica. *Geology*, 31:
632 107-110.

633 Barker, P.F., 1982. The Cenozoic subduction history of the Pacific margin of the
634 Antarctic Peninsula: Ridge crest-trench interactions. *J. Geol. Soc.*, 139: 787-
635 801.

636 BAS, 1995. James Ross Island 1:100,000. British Antarctic Territory Topographic
637 Maps: BAS 100 Series. British Antarctic Survey, Cambridge

638 Behrendt, J.C., Finn, C.A., Blankenship, D., and Bell, R.E., 1998. Aeromagnetic
639 evidence for a volcanic caldera(?) complex beneath the divide of the West
640 Antarctic Ice Sheet. *Geophys. Res. Lett.*, 25: 4385-4388.

641 Bell, R., Blankenship, D.D., Finn, C.A., Morse, D.L., Scambos, T.A., Brozena, J.M.,
642 and Hodge, S.M., 1998. Influence of subglacial geology on the onset of a West
643 Antarctic ice stream from aerogeophysical observations. *Nature*, 394: 58-62.

644 Bell, R.E., Childers, V.A., Arko, R.A., Blankenship, D.D., and Brozena, J.M., 1999.
645 Airborne gravity and precise positioning for geologic applications. *J. Geophys.*
646 *Res.*, 104: 15281-17292.

- 647 Blakely, R.J., 1995. Potential Theory in Gravity and Magnetic Applications.
648 Cambridge University Press, Cambridge.
- 649 Blankenship, D.D., Bell, R.E., Hodge, S.M., Brozena, J.M., Behrendt, J.C., and Finn,
650 C.A., 1993. Active volcanism beneath the West Antarctic ice sheet and
651 implications for ice-sheet stability. *Nature*, 361: 526-529.
- 652 Chevallier, L., Verwoerd, W.J., Bova, P., Stettler, E., Du Plessis, A., Du Plessis, J.G.,
653 Fernandez, L.M., and Nel, M., 1992. Volcanological features and preliminary
654 geophysical investigations on Marion Island. *S. Afr. J. Antarct. Res.*, 22: 15-
655 35.
- 656 Childers, V.A., McAdoo, D., Brozena, J., and Laxon, S., W., 2001. New gravity data
657 in the Arctic. *Ocean: Comparison of airborne and ERS gravity. J. Geophys.*
658 *Res.*, 106: 8871-8886.
- 659 Corr, H., and Vaughan, D.G., 2008. A recent volcanic eruption beneath the West
660 Antarctic ice sheet. *nature geoscience* In press.
- 661 del Valle, R.A., Díaz, M.T., Febrer, J.M., and Keller, M.A., 1992. Estudio sísmico en
662 la isla James Ross. In: C.A. Rinaldi (Editor). *Geología de la isla James Ross.*
663 *Dirección Nacional del Antártico. Instituto Antártico Argentino, Buenos Aires,*
664 *315-322 pp.*
- 665 Dufek, J., and Bergantz, G.W., 2005. Lower Crustal Magma Genesis and
666 Preservation: a Stochastic Framework for the Evaluation of Basalt–Crust
667 Interaction. *Journal of Petrology*, 46: 2167–2195
668 doi:10.1093/petrology/egi049.
- 669 Elliot, D.H., 1998. Tectonic setting and evolution of the James Ross Basin, northern
670 Antarctic Peninsula. *Geol. Soc. Am. Mem.*, 169: 541-555.

- 671 Ferraccioli, F., Armadillo, A., Bozzo, E., and Privitera, E., 2000. Magnetism and
672 gravity image tectonic framework of the Mount Melbourne Volcano area
673 (Antarctica). *Phys. Chem. Earth*, 25: 387-393.
- 674 Ferraccioli, F., Jones, P.C., Curtis, M.L., and Leat, P.T., 2005. Subglacial imprints of
675 early Gondwana break-up as identified from high resolution aerogeophysical
676 data over western Dronning Maud Land, East Antarctica. *Terra Nova*, 17:
677 573–579.
- 678 Ferraccioli, F., Jones, P.C., Vaughan, A.P.M., and Leat, P.T., 2006. New
679 aerogeophysical view of the Antarctic Peninsula: More pieces, less puzzle.
680 *Geophys. Res. Lett.*, 33: doi:10.1029/2005GL024636.
- 681 Finn, C.A., and Morgan, L.A., 2002. High-resolution aeromagnetic mapping of
682 volcanic terrain, Yellowstone National Park. *J. Volcanol. Geoth. Res.*, 115:
683 207-231.
- 684 Garrett, S.W., 1990. Interpretation of reconnaissance gravity and aeromagnetic
685 surveys of the Antarctic Peninsula. *J. Geophys. Res.*, 95: 6759-6777.
- 686 GRAV3D; A Program Library for Forward Modelling and Inversion of Gravity Data
687 over 3D Structures, version 3.0 (2006). Developed under the consortium
688 research project Joint/Cooperative Inversion of Geophysical and Geological
689 Data. UBC-Geophysical Inversion Facility, Department of Earth and Ocean
690 Sciences, University of British Columbia, Vancouver, British Columbia.
- 691 Hambrey, M.J., Smellie, J.L., Nelson, A.E., and Johnson, J.S., 2008. Late Cenozoic
692 glacier-volcano interaction on James Ross Island and adjacent areas, Antarctic
693 Peninsula region. *GSA Bul.* doi: 10.1130/B26242.1.
- 694 Harlan, R.B., 1968. Eotvos corrections for airborne gravity. *J. Geophys. Res.*, 73:
695 4675 - 4679.

- 696 Hole, M.J., and Larter, R.D., 1993. Trench-proximal volcanism following ridge crest-
697 trench collision along the Antarctic Peninsula. *Tectonics*, 12: 897-910.
- 698 Hole, M.J., Rogers, G., Saunders, A.D., and Storey, M., 1991. Relation between
699 alkalic volcanism and slab-window formation. *Geology*, 19: 657-660.
- 700 Hole, M.J., Saunders, A.D., Rogers, G., and Sykes, M.A., 1992. The relationship
701 between alkaline magmatism, lithospheric extension and slab window
702 formation along continental destructive plate margins. In: J.L. Smellie
703 (Editor). *Volcanism associated with extension at consuming plate margins*.
704 *Spec. Publ., . Geol. Soc., Lond*, 81, 265-285 pp.
- 705 Hole, M.J., Saunders, A.D., Rogers, G., and Sykes, M.A., 1995. The relationship
706 between alkaline magmatism, lithospheric extention and slab window
707 formation along continental destructive plate margins. *J. Geol. Soc.*, 81: 265-
708 285.
- 709 Holt, J.W., Richter, T.G., Kempf, S.D., and Morse, D.L., 2006. Airborne gravity over
710 Lake Vostok and adjacent highlands of East Antarctica. *G-cubed*, 7:
711 doi:10.1029/2005GC001177.
- 712 Horgana, H., Naishb, T., Bannisterb, S., Balfoura, N., and Wilson, G., 2005. Seismic
713 stratigraphy of the Plio-Pleistocene Ross Island flexural moat-fill: a prognosis
714 for ANDRILL Program drilling beneath McMurdo-Ross Ice Shelf. *Global*
715 *Planet Change*, 45: 83–97.
- 716 Janik, T., Środa, P., Grad, M., and Aleksander Guterch, A., 2006. Moho Depth along
717 the Antarctic Peninsula and Crustal Structure across the Landward Projection
718 of the Hero Fracture Zone. In: D. Karl Fütterer, D. Damaske, G. Kleinschmidt,
719 H. Miller and F. Tessensohn (Editors). *Antarctica Contributions to Global*
720 *Earth Sciences*. Springer Berlin Heidelberg, 229-236 pp.

- 721 Jones, P.C., and Johnson, A.C., 1995. Airborne gravity survey in southern Palmer
722 Land, Antarctica. In: K.P. Schwarz, J. Brozena and G. Hein (Editors).
723 Proceedings of IAG Symposium on Airborne Field Determination.
724 Department of Geomatics Engineering at the University of Calgary, Calgary,
725 Alberta, Canada, IUGG XXI General Assembly, Boulder, Colorado, 117-123
726 pp.
- 727 Jones, P.C., Johnson, A.C., von Frese, R.R.B., and Corr, H., 2002. Detecting rift
728 basins in the Evans Ice Stream region of West Antarctica using airborne
729 gravity data. *Tectonophysics*, 347: 25-41.
- 730 Jordan, T.A., Ferraccioli, F., Corr, H., Robinson, C., Caneva, G., Armadillo, A.,
731 Bozzo, E., and Frearson, N., 2007. Linking the Wilkes Subglacial Basin, the
732 Transantarctic Mountains, and the Ross Sea with a New Airborne Gravity
733 Survey. *Terra Antarctica Reports*, 13: 18pp.
- 734 LaBrecque, J.L., and Ghidella, M.E., 1997. Bathymetry, depth to magnetic basement,
735 and sediment thickness estimates from aerogeophysical data over the western
736 Weddell Basin. *J. Geophys. Res.*, 102: 7929–7946.
- 737 LaCoste, L.J.B., 1967. Measurement of gravity at sea and in the air. *Rev. Geophys.*, 5:
738 477-526.
- 739 Larter, R.D., and Barker, P.F., 1991. Effects of ridge crest-trench interaction on
740 Antarctic-Phoenix spreading: Forces on a young subducting plate. *J. Geophys.*
741 *Res.*, 96: 19583-19607.
- 742 Lehman, J.A., Smith, R.B., Schilly, M.M., and Braile, L.W., 1982. Upper crustal
743 structure of the Yellowstone Caldera from seismic delay time analyses and
744 gravity correlations. *J. Geophys. Res.*, 87: 2713-2730.

- 745 LeMasurier, W.E., and Thomson, J.W. (Editors). 1990. Volcanoes of the Antarctic
746 Plate and Southern Oceans. Antarctic Research Series, 48. American
747 Geophysical Union, Washington, D.C, 512 pp.
- 748 Lemoine, F.G., Kenyon, S.C., Factor, J.K., Trimmer, R.G., Pavlis, N.K., Chinn, D.S.,
749 Cox, C.M., Klosko, S.M., Luthcke, S.B., Torrence, M.H., Wang, Y.M.,
750 Williamson, R.G., Rapp, R.H., and Olson, T.R., 1998. The development of the
751 joint NASA/GSFC and the National Imagery and Mapping Agency (NIMA)
752 geopotential models, EGM96, . Report No TP-1998-206861, NASA.
- 753 Li, Y., and Oldenburg, D.W., 1998. 3-D inversion of gravity data. *Geophysics*, 63:
754 109-119.
- 755 Lythe, M.B., Vaughan, D.G., and the-BEDMAP-Consortium, 2000. BEDMAP – bed
756 topography of the Antarctic. British Antarctic Survey, Cambridge,
757 1:10,000,000 scale map pp.
- 758 Mader, G.L., 1992. Rapid static and kinematic global positioning system solutions
759 using the ambiguity function technique. *J. Geophys. Res.*, 97: 3271-3283.
- 760 Masturyono, McCaffrey, R., Wark, D.A., Roecker, S.W., Fauzi, Ibrahim, G., and
761 Sukhyar., 2001. Distribution of magma beneath the Toba caldera complex,
762 north Sumatra, Indonesia, constrained by three-dimensional P wave velocities,
763 seismicity, and gravity data. *G-cubed*, 2: 1527-2027.
- 764 McCarron, J.J., and Larter, R.D., 1998. Late Cretaceous to early Tertiary subduction
765 history of the Antarctic Peninsula *J. Geol. Soc.*, 155: 255-268.
- 766 Nelson, P.H.H., 1975. The James Ross Volcanic Group of north-east Graham Land.
767 British Antarctic Survey Scientific reports, 54: 62pp.

- 768 Oehler, J.F., Van Wyk de Vries, B., and Labazuy, P., 2005. Landslides and spreading
769 of oceanic hot-spot and arc shield volcanoes on Low Strength Layers (LSLs):
770 an analogue modeling approach. *J. Volcanol. Geoth. Res.*, 144: 169-189.
- 771 Philpotts, A.R., and Dickson, L.D., 2000. The formation of plagioclase chains during
772 convective transfer in basaltic magma. *Nature*, 406: 59-61.
- 773 Robertson, S.D., Wiens, D.A., and P.J., S., 2003. Seismicity and tectonics of the
774 South Shetland Islands and Bransfield Strait from a regional broadband
775 seismograph deployment. *J. Geophys. Res.*, 108: doi:10.1029/2003JB002416.
- 776 Skilling, I.P., 2002. Basaltic pahoehoe lava-fed deltas: large-scale characteristics, clast
777 generation, emplacement processes and environmental discrimination. In: J.L.
778 Smellie and M.G. Chapman (Editors). *Volcano—ice interaction on Earth and*
779 *Mars. Spec. Publ. Geol. Soc., Lond.*, 202, 91-113 pp.
- 780 Sloan, B.J., Lawver, L., and Anderson, J.B., 1995. Seismic stratigraphy of the Larsen
781 Basin, eastern Antarctic Peninsula. *Antarctic Research Series*, 68: 59-74.
- 782 Smellie, J.L., 1987. Geochemistry and tectonic setting of alkaline volcanic rocks in
783 the Antarctic Peninsula: a review. *J. Volcanol. Geoth. Res.*, 32: 269-285.
- 784 Smellie, J.L., 1999. Lithostratigraphy of Miocene-Recent, alkaline volcanic fields in
785 the Antarctic Peninsula and eastern Ellsworth Land. *Antarct. Sci.*, 11: 362-
786 378.
- 787 Smellie, J.L., 2006. The relative importance of supraglacial versus subglacial
788 meltwater escape in basaltic subglacial tuya eruptions: an important
789 unresolved conundrum. *Earth-Science Reviews*, 74: 241-268.
- 790 Smellie, J.L., Johnson, J.S., McIntosh, W.S., Esser, R., Gudmundsson, M.T.,
791 Hambrey, M.J., and van Wyk de Vries, B., 2008. Six million years of glacial

- 792 history recorded in the James Ross Island Volcanic Group, Antarctic
793 Peninsula. Palaeogeography, Palaeoclimatology, Palaeoecology In press.
- 794 Stern, T.A., Davey, F.J., and Delisle, G., 1991. Lithospheric flexure induced by the
795 load of the Ross Archipelago, southern Victoria land, Antarctica. In: M.R.A.
796 Thomson, A. Crame and J.W. Thomson (Editors). Geological evolution of
797 Antarctica. Cambridge University Press, 323-328 pp.
- 798 Strelin, J.A., 1995. Interpretación de secuencias sísmicas en la plataforma
799 noroccidental del mar de Weddell (cuenca Larsen), Antártida. Terceras
800 Jornadas de Comunicaciones Antárticas, Instituto Antártico Argentino.
- 801 Studinger, M., Bell, R., and Tikku, A.A., 2004. Estimating the depth and shape of
802 subglacial Lake Vostok's water cavity from aerogravity data. Geophys. Res.
803 Lett., 31: doi:10.1029/2004GL019801.
- 804 Studinger, M., Bell, R.E., Karner, G.D., Tikku, A.A., Holt, J.W., Morse, D.L.,
805 Richter, T.G., Kempf, S.D., Peters, M.E., Blankenship, D.D., Sweeney, R.E.,
806 and Rystrom, V.L., 2003. Ice cover, landscape setting, and geological
807 framework of Lake Vostok, East Antarctica. Earth Planet. Sci. Lett., 205: 195-
808 210.
- 809 Studinger, M., Bell, R.E., Buck, W.R., Karner, G.D., Blankenship, D.D., 2004. Sub-
810 ice geology inland of the Transantarctic Mountains in light of new
811 aerogeophysical data. Earth Planet. Sci. Lett., 220: 391-408.
- 812 Swain, C.J., 1996. Horizontal acceleration corrections in airborne gravimetry.
813 Geophysics, 61: 273-276.
- 814 Sykes, M.A., 1989. The petrology and tectonic significance of the James Ross Island
815 Volcanic Group, University of Nottingham, 218 pp.

- 816 Tibaldi, A., 2004. Major changes in volcano behaviour after a sector collapse: insights
817 from Stromboli, Italy. *Terra Nova*, 16: doi: 10.1046/j.1365-
818 3121.2003.00517.x.
- 819 van Wyk de Vries, B., Ferrari, L., and Pasquarè, G., 1992. Importance o gravitational
820 spreading in the tectonic and volcanic evolution of Mount Etna. *Nature*, 357:
821 231-235.
- 822 van Wyk de Vries, B., and Francis, P.W., 1997. Catastrophic collapse at
823 stratovolcanoes induced by gradual volcano spreading. *Nature*, 387: 387-390.
- 824 van Wyk de Vries, B., and Matela, R., 1998. Styles of volcano-induced deformation:
825 Numerical models of substratum flexure, spreading, and extrusion. *J.*
826 *Volcanol. Geoth. Res.*, 81: 1-18.
- 827 von Frese, R.R.B., Hinze, W.J., Braile, L.W., and Luca, A.J., 1981. Spherical earth
828 gravity and magnetic anomaly modeling by Gauss- Legendre quadrature
829 integration. *J. Geophys*, 49: 234-242.
- 830 von Frese, R.R.B., and Mateskon, S.R., 1985. Modelling magnetic and gravity effects
831 of the Transantarctic Mountains. *Antarctic Journal of the United States*, XX:
832 1-3.
- 833 Walker, G.P.L., 1989. Gravitational (density) controls on volcanism, magma
834 chambers and intrusions. *Aust. J. Earth. Sci.*, 36: 149-165.
- 835 Watts, A.B., 2001. *Isostasy and Flexure of the lithosphere*. Cambridge University
836 Press, Cambridge, 458 pp.
- 837 Watts, A.B., and Stewart, J., 1998. Gravity anomalies and segmentation of the
838 continental margin offshore Gabon, West Africa. *Earth Planet. Sci. Lett.*, 156:
839 239-252.

840 Wessel, P., and Smith, W.H.F., 1991. Free software helps map and display data. *Eos*
841 *Trans. AGU*, 72: 441.

842 Whitham, A.G., 1988. Syn-depositional deformation in a Cretaceous succession,
843 James Ross Island, Antarctica. Evidence from vitrinite reflectivity. *Geol. Mag.*,
844 125: 583-591.

845 Woollard, G.P., 1979. The new gravity system - Changes in international gravity base
846 values and anomaly values. *Geophysics*, 44: 1352-1366.

847

848

849 **Figure 1.** Location map of the aerogravity survey in the James Ross Island region
850 (dashed box), and major regional tectonic elements. Hatched region marks
851 Larsen/James Ross basin (Robertson et al., 2003). Black ovals mark location of alkali
852 basaltic volcanic outcrops (Smellie, 1999).

853 **Figure 2.** Topography and airborne gravity data. a) Surface topography across the
854 James Ross Island region and aerogeophysical survey line locations (grey:
855 aeromagnetic; black: aerogravity and aeromagnetic). b) Sub-ice topography. c) Free-
856 air gravity anomaly. d) Bouguer gravity anomaly based on a correction density of
857 2670 kgm^{-3} . White lines show the outcrop of Cretaceous sediments underlying the
858 JRIVG (Nelson, 1975). Dotted grey line shows extent of short-wavelength
859 aeromagnetic anomalies. Grey areas mark location of highest amplitude aeromagnetic
860 anomalies. Black line shows location of profile A-A'.

861

862 **Figure 3.** Profile A-A' across James Ross Island (profile location shown in Fig. 2d).
863 a) Solid lines show Bouguer anomaly based on correction densities between 2670 and
864 2270 kgm^{-3} . Thick solid line shows Bouguer anomaly with preferred correction

865 density of 2470 kgm^{-3} . Dashed lines show simple Airy isostatic anomaly, assuming
 866 the compensation scheme shown in Figure 4a. Moho depths of 22 km (long dashed
 867 line), or 35 km (dotted line) were assumed. b) Surface topography (solid line) and
 868 flexural surfaces due to loading of the Mt Haddington volcanic edifice for T_e values
 869 of 0, 1, 2, 4, 8 and 16 km (dashed lines). Arrows mark the load edges. c) Calculated
 870 flexural gravity anomalies (dashed lines) assuming the crustal model shown in Figure
 871 4b.

872

873 **Figure 4.** Cartoons illustrating different types of compensation depending on crustal
 874 structure. a) Simple Airy compensation, with thicker than average crust beneath
 875 elevated topography and thinned crust across the ocean-continent transition. In this
 876 case load density = crustal density and the calculated gravity anomaly arises only
 877 from deflections of the Moho. T_i = initial crustal thickness. b) Flexural compensation,
 878 associated with elastic support of the surface load and the development of a flexural
 879 moat. In this model the calculated gravity anomaly arises from both the flexural basin
 880 infill and the Moho effect.

881

882 **Figure 5.** Density structure from GRAV3D inversion applied to the observed
 883 Bouguer gravity anomaly over James Ross Island: a) Perspective view of the study
 884 region looking NE; b) shows selected bodies with apparent density contrasts greater
 885 than $\pm 30 \text{ kgm}^{-3}$ with respect to background; c) E—W section; d) N—S section.

886

887 **Figure 6.** Results for constrained inversion along section A-A' (location shown in
 888 Fig. 2d). a) Caldera-like model after 0 to 8 iterations (light grey to black broken
 889 lines). Top of caldera-like body (solid line) at 0 m. b) Calculated gravity anomalies

890 (broken lines) for the caldera-like model. Solid line shows the observed Bouguer
891 gravity anomaly assuming a correction density of 2470 kgm^{-3} ; c) Magma chamber
892 model after 0 to 8 iterations. Top of the magma chamber body at 5 km; d) Calculated
893 Bouguer gravity anomalies for the magma chamber model.

894

895 **Figure 7.** Interpretative cross-section for James Ross Island, showing volcanic
896 loading inducing viscous flow of sediments (grey) beneath an elasto-plastic lid (dark
897 grey). The volcanic pile is shown with V ornaments, while H ornamented region
898 depicts deep rocks in a volcanic “root” that may have been geothermally altered.
899 Region of T ornament represents possible low-density tuff material, which may
900 further reduce the density beneath the summit of the volcano.

901

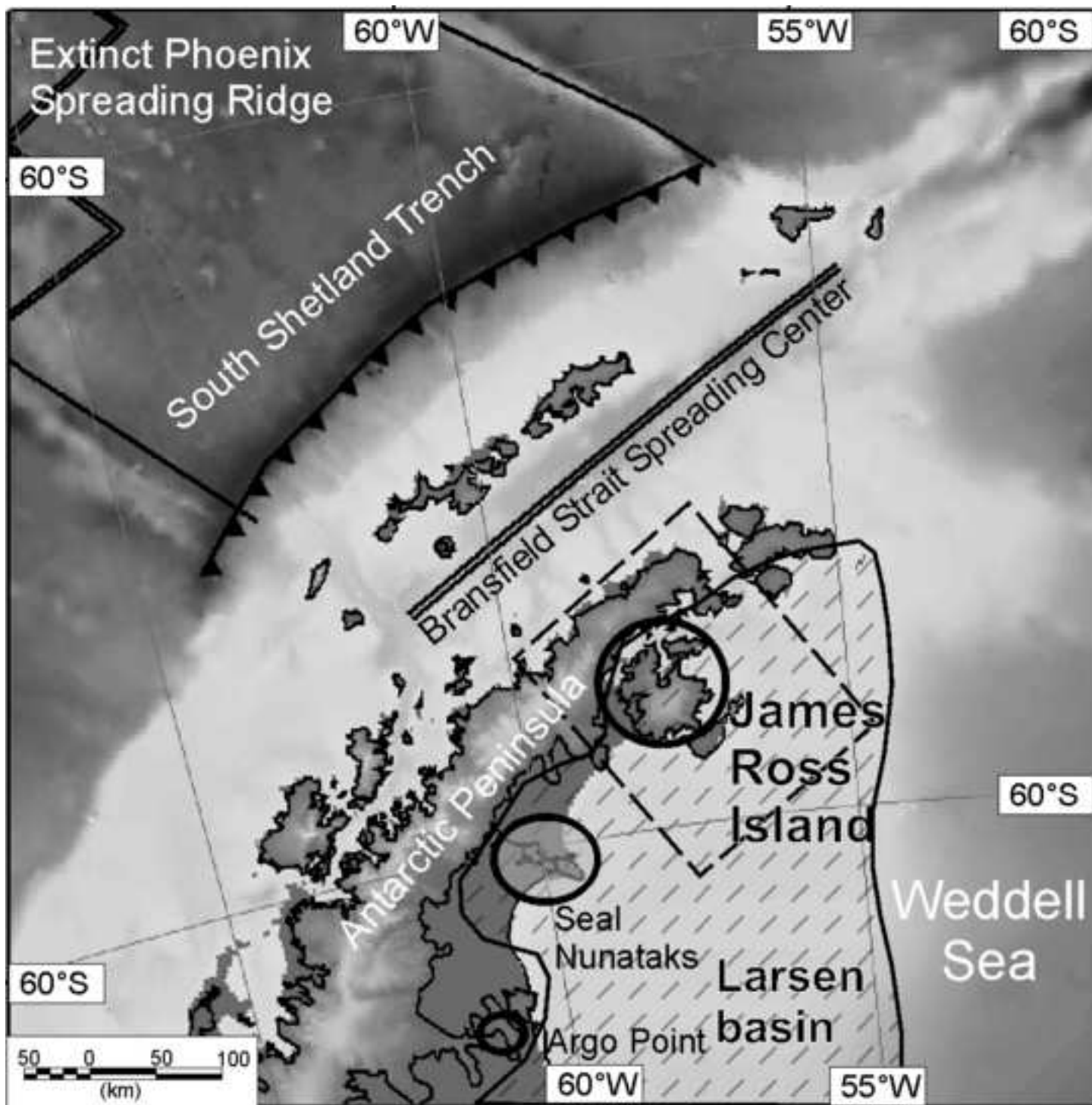
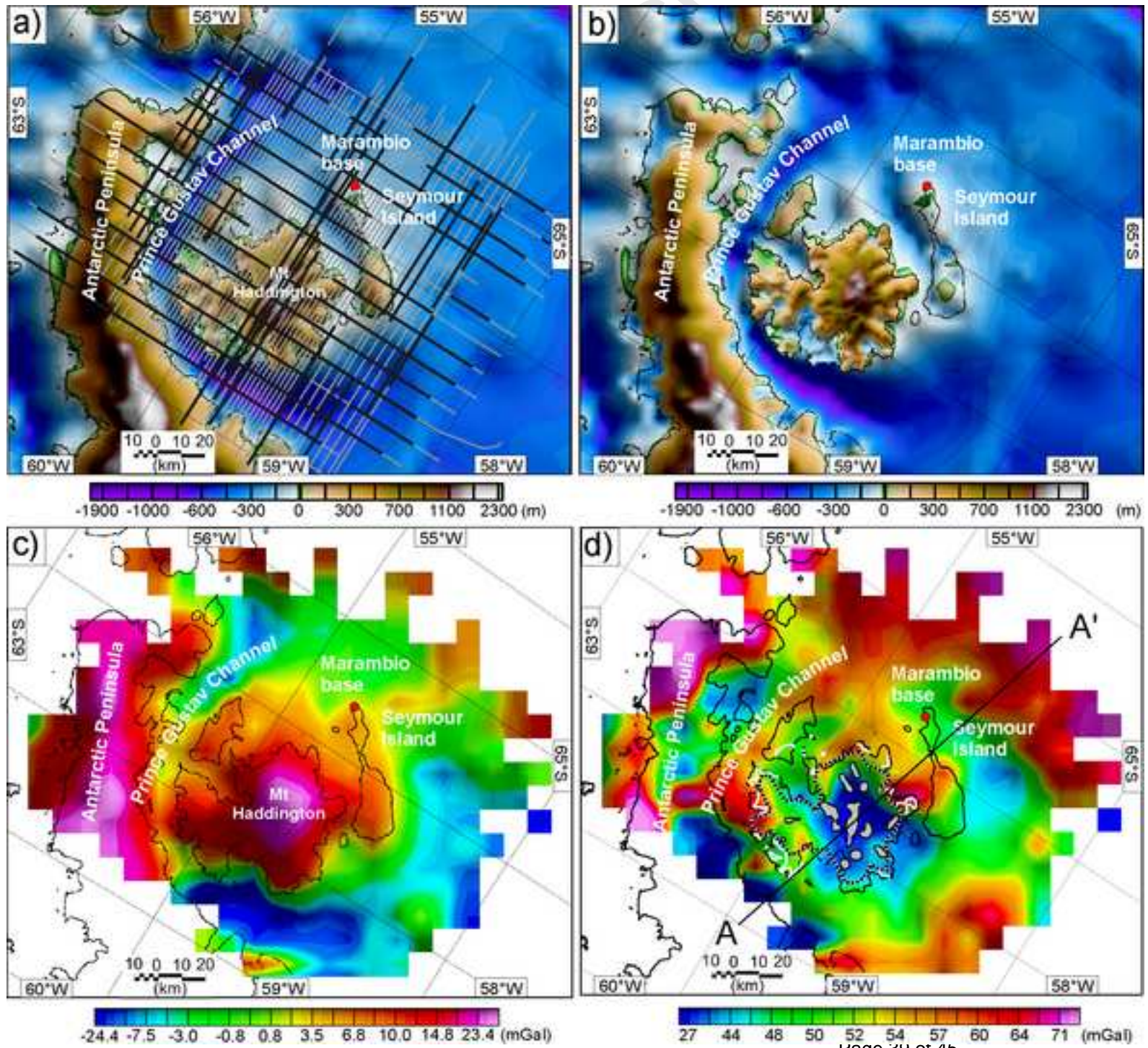
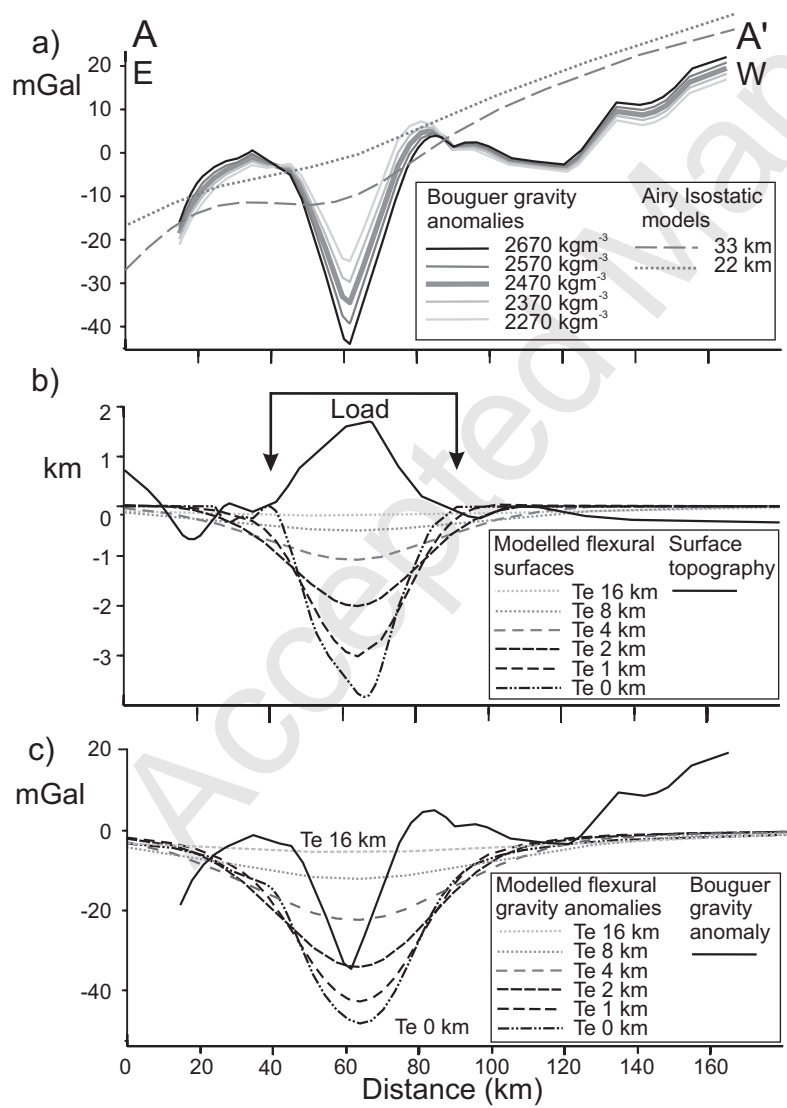
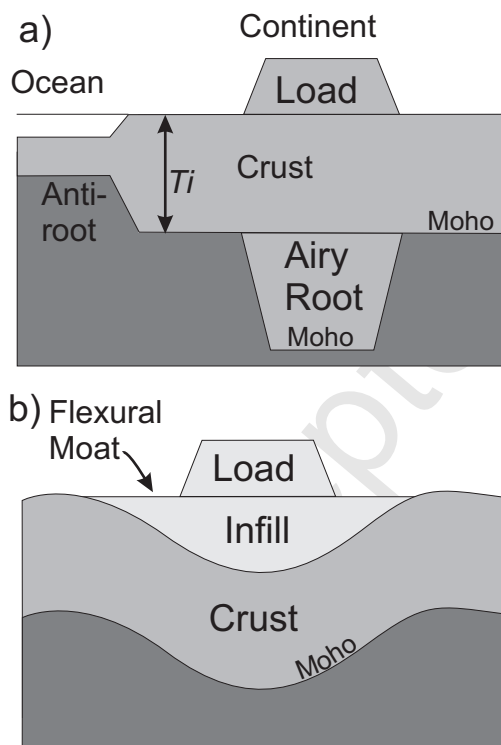


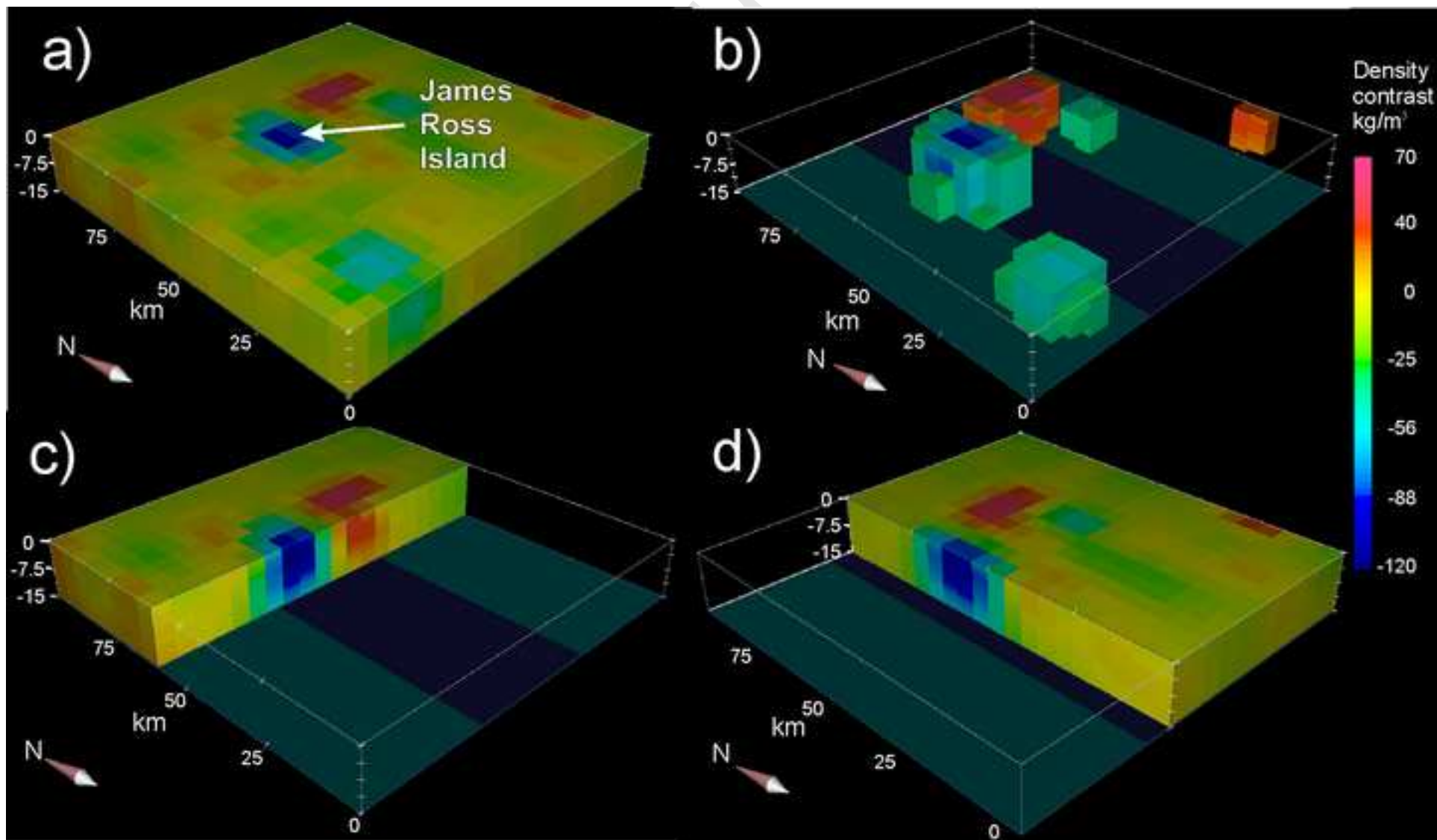
Figure2







Manuscript



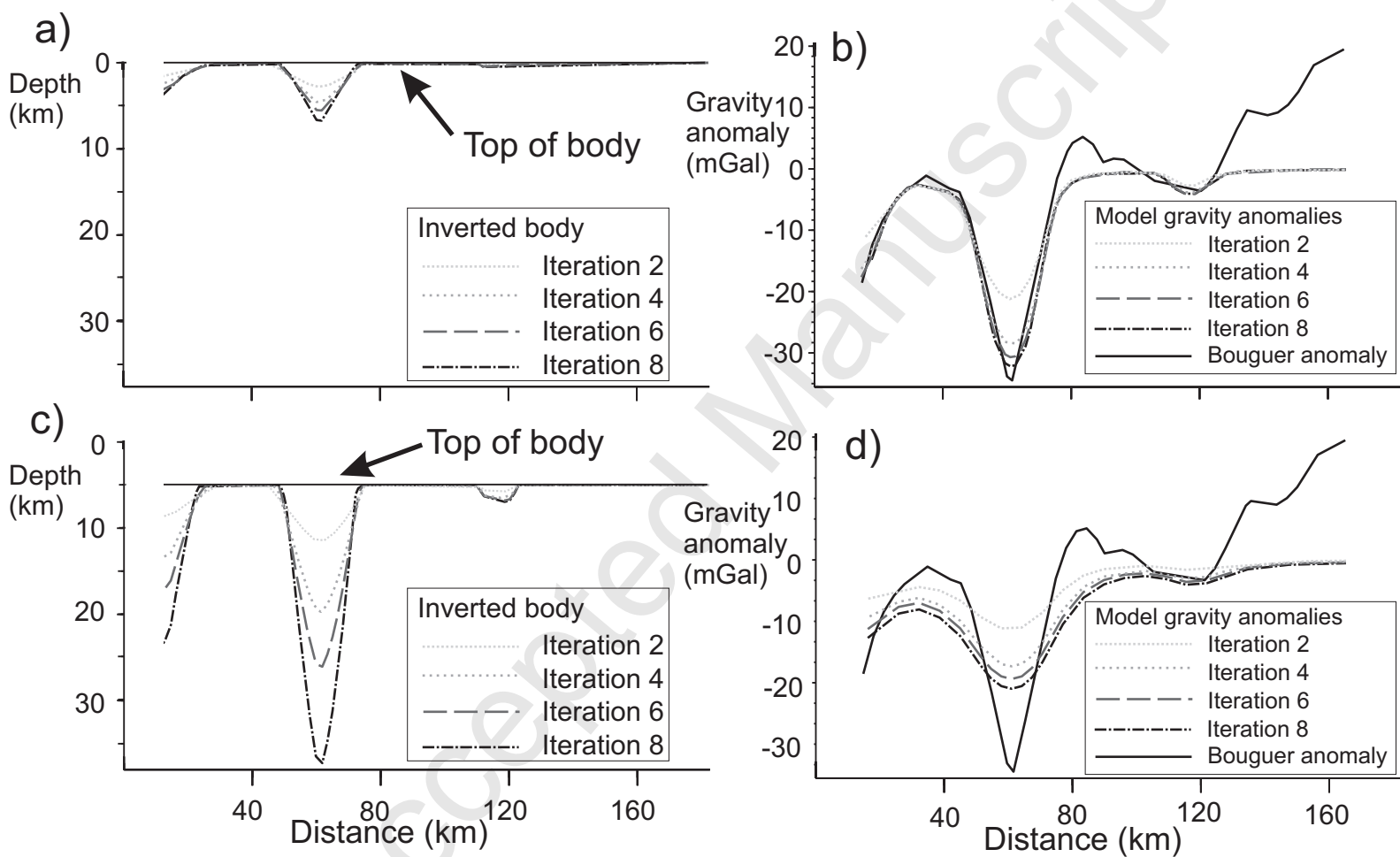


Figure 7

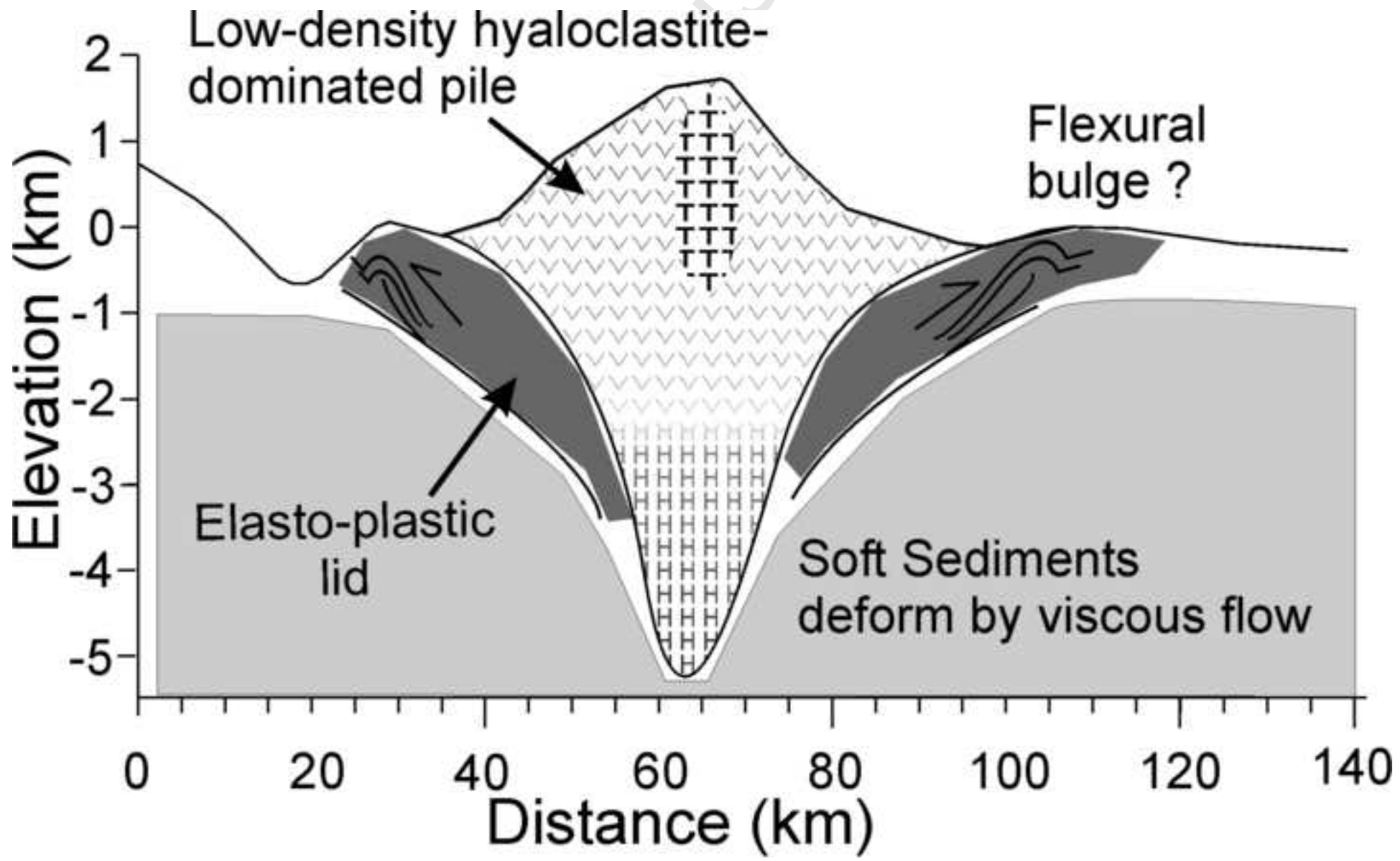


Table 1. Rock densities (Gudmundsson, pers. com.) and proportions (Smellie et al., 2008) making up the volcanic edifice on James Ross Island.

Lithology	Average Density (kgm^{-3})	Percent
Basalt lava	2780	30
Hyaloclastite	2380	65
Tuff	1810	5
Bulk density	2470	

Accepted Manuscript